Functionalization of Boron Nitride Nanosheets by Diazonium Salt for Preparation of Nanocomposites With High-Density Polyethylene

Zhujun Wang,[1,2] Qian Li,[1] Zheming Chen,[1] Huayi Li,[1]* Shuirong Zheng,[2] Xiaobin Tang[3]

[1]*Beijing National Laboratory for Molecular Sciences, CAS Key Laboratory of Engineering Plastics Institute of Chemistry, Chinese Academy of Sciences, Beijing, 100190, China*

[2]*Key Laboratory of Space Applied Physics and Chemistry, Ministry of Education, Northwestern Polytechnical University, Xi'an, Shaanxi, 710129, People's Republic of China*

[3]*Nanjing University Aeronaut & Astronaut, Department of Nuclear Science & Engineering, Nanjing, 210016, Jiangsu, Peoples Republic of China*

Functionalization of boron nitride nanosheets (BNNSs) has always been a challenge due to its chemical inertness and anti-oxidative properties. In a concentrated base environment, the B-N bonds on the surface of BNNSs were broken to produce a large number of B-OH and N-H functional groups. Afterwards, aniline carbocation produced by decomposition of the diazonium salt was utilized to achieve high grafting content of Ph-NH_2 groups onto the surface of BNNSs. Further, the amide reaction between amino and stearyl chloride verified the reactivity of Ph-NH_2 groups on the surface of BNNSs, with the result that BNNSs were abundantly decorated by aliphatic chains at 22.9 wt% grafting yield. The surface aliphatic chains of BNNSs strongly improved the interfacial adhesion between the High-density polyethylene (HDPE) matrix and the filler and provided an excellent dispersion of SC-BNNSs in the HDPE matrix. Therefore, HDPE/SC-BNNSs nanocomposites showed improved thermal stability, thermal conductivity, neutron shielding property and flexural modulus with no apparent reduction in tensile strength. When filler content exceeded 5 wt%, the HDPE/SC-BNNSs nanocomposites showed a higher thermal decomposition temperature than the composites with pristine BNNSs fillers. POLYM. COMPOS., 40:2346–2356, 2019. © 2018 Society of Plastics Engineers

INTRODUCTION

The demand for reliable radiation shielding materials has been growing since the last decade [1,2]. Polymer composites with fillers containing ^{10}B elements can effectively shield against the neutron radiation [3,4]. In particular, High-density polyethylene (HDPE) composites containing B are generally used for this purpose [5]. HDPE, possessing a high content of hydrogen atoms, plays as a mighty polymeric neutron moderator through its large scattering power [6]. Boric compounds are relatively cheap and have an excellent thermal neutron absorption ability. Especially, compared with micro-sized ^{10}B containing fillers, nano-sized fillers could lead to a better thermal neutron absorption efficiency of the composite [7,8]. However, the high surface energy of nano-sized particles decreases their interfacial adhesion with the polymer matrix and makes them easy to form agglomerates [9]. In this aspect, it is necessary to achieve the surface modification of ^{10}B containing nanoparticles to improve their dispersibility in the polymer matrix.

Hexagonal boron nitride nanosheets (h-BNNSs) have an excellent thermal neutron absorption ability because of ^{10}B atoms [10]. In addition, it is also widely used as thermally conductive material owing to the high thermal conductivity of 60 $W{\cdot}m^{-1}{\cdot}K^{-1}$. However, the high chemical inertness and anti-oxidative properties of h-BNs make its functionalization quite difficult. Practical applications of h-BNs nanomaterials were severely limited by their high surface energy and strong tendency to aggregate in the HDPE matrix, which were fatal to properties of polymer composites [11].

At present, there were several kinds of methods for surface modification of h-BNs, including non-covalent

Correspondence to: H. Li; e-mail: lihuayi@iccas.ac.cn
Contract grant sponsor: National Science Foundation of China; contract grant number: 51403216. contract grant sponsor: Seed Foundation of Innovation and Creation for Graduate Students in Northwestern Polytechnical University; contract grant number: 2017207.
DOI 10.1002/pc.25093
Published online in Wiley Online Library (wileyonlinelibrary.com).

modification, covalent modification and solid-state surface modification. Among them, the limited scalability is the main drawback of non-covalent processes. Meanwhile, the bonding between non-covalent modifiers and h-BNs is usually not as strong and stable as that in covalent modifications [12]. For example, silane agents can be used to form non-covalent coatings on the surface of h-BNs. Xu and Chung [13] used Dow Corning Z-6040 Silane to treat the surface of h-BN filler in order to improve the affinity between filler and epoxy matrix, but it was easy to peel the coating layer from h-BNs. As for solid-state surface modification, thermal treatment [14–16] and high-energy radiation [17,18] were the most common methods. These methods introduced hydroxyl or amino groups onto h-BNs, but mostly were energy-intensive and inefficient. As for covalent modification, due to the good chemical stability of BNNSs, existing modification methods are often not quite effective to break the B-N bonds. Sainsbury et al. [19] presented a covalent approach for functionalization of BNNSs by using oxygen radicals. BNNSs were mixed with organic peroxide under at high temperatures and pressures to introduce hydroxyl groups. The obvious disadvantage of this method was that the reaction condition was harsh. There were also reports to disperse h-BNs into NaOH solutions and introduce the -OH on the surface of h-BNs thus to improve the dispersibility of h-BNs in the epoxy matrix for thermal conductivity and improved mechanical properties [20,21]. However, the practical application of the h-BNs would still be limited in nonpolar organic polymers. Therefore, an effective method to break the B-N bond and decorate a high density of functional groups on BNNSs remained to be developed [22].

As an application of boron nitride, Jan et al. [23] used liquid exfoliation of hexagonal Boron-Nitride (BN) to prepare polyvinylchloride composites of different-size BN nanosheets with more excellent mechanical properties than that of the pristine polymer. Yi et al. [24–26] proposed a novel and effective hydrodynamics method to realize large-scale production of BNNSs with much higher yield and efficiency, which could be utilized as fillers or coatings to protect polymer from oxygen-atom corrosion. Harrison et al. [27] used trifunctional alkoxysilane loaded on boron nitride to improve its dispersion in the HDPE matrix to enhance the neutron shielding performance of the composite, but the effect was improved but not significant. Zhang et al. [28] made an effective neutron shielding material by alternating multi-layered containing BN composites. The probability of collision between incident photons and flake-shaped particles was enhanced through alignment of the oriented BN particles, thus neutron transmittance noticeably decreased with an increasing number of layers. However, this method did not improve the dispersion of BN in HDPE. Therefore, we hope to find a solution that can not only promote the dispersion of BN in HDPE matrix, but also significantly improve the neutron shielding effect of HDPE/BN composites.

In this study, we proposed an innovative and simple approach to impart BNNSs a large number of B-OH and N-H functional groups. Afterwards, the high activity of carbon-positive irons produced by diazonium salt hydrolysis was utilized to graft Ph-NH_2 onto the surface of HO-BNNSs. As an example, the amide reaction between amino and stearyl chloride verified the reactivity of the -NH_2 groups grafted on the surface of BNNSs. Additionally, aliphatic chain modified BNNSs/HDPE nanocomposites were fabricated through conventional melt-extrusion. The mechanical property, thermal stability, thermal conductivity, and neutron shielding property of HDPE/SC-BNNSs nanocomposites were investigated and compared with HDPE/BNNSs nanocomposites and neat HDPE to illustrate the advantage of the surface modified BNNSs.

EXPERIMENTAL

Materials

HDPE was purchased from Beijing Yanshan Petrochemical Co., Ltd. h-BNNSs, stearyl chloride and pyridine were purchased from Aladdin reagent (Shanghai) co. LTD. The reagents used for the synthesis of benzene diazonium chloride, including p-phenylenediamine, sodium nitrite ($NaNO_2$), concentrated hydrochloric acid (HCl) and iron powder were purchased from J&K Scientific Ltd. All chemicals and reagents were used directly without further purification. Deionized water was generated by a Milli-Q integral ultrapure water purification system.

Surface Chemical Functionalization of BNNSs

Synthesis of HO-BNNSs. Hydroxylation treatment of BNNSs was conducted and the method was based one reported process [16]. In a concentrated base environment, the B-N bonds were broken by this high-temperature solid-phase method to produce a large number of B-OH and N-H groups. First,1 g BNNSs, 2.8-g sodium hydroxide and 2.8-g potassium hydroxide were co-grounded and mixed. Then the mixed powder was moved to the hydrothermal reactor. The reaction was conducted at 180°C for 5 h, following 1-h ultrasonic treatment. Finally, the product was centrifuged, purified and named as HO-BNNSs. The scheme was shown as Fig. 1.

Synthesis of A-BNNSs. The high activity of aniline-carbocation produced by decomposition of diazonium salt was utilized to graft Ph-NH_2 onto the surface of HO-BNNSs. Detail procedure was given as follow. First, 1.6 g p-phenylenediamine was dissolved in 20 mL deionized water with an ice bath (<5°C). Then 11 mL 0.5 mol·mL^{-1} HCl was added dropwise under stirring to form amaranth suspension. Afterward, 1.02 g $NaNO_2$ dissolved in aqueous solution was slowly added to generate the diazonium chloride salt. Subsequently, the diazonium salt solution was

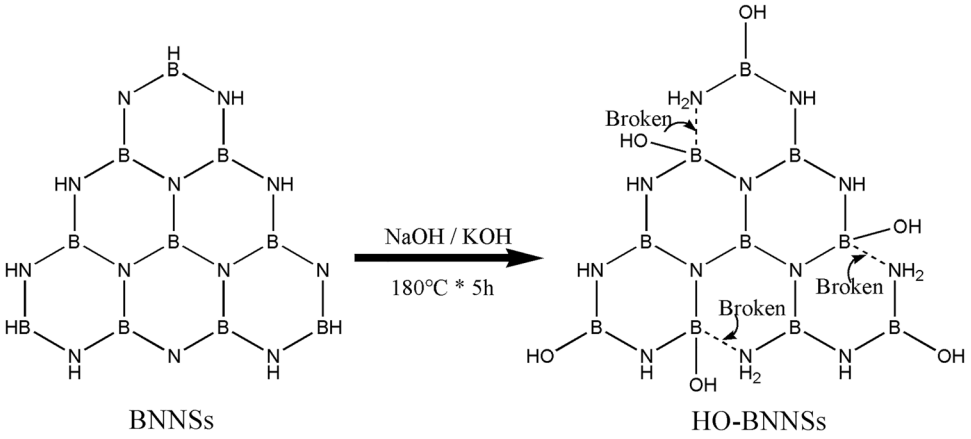

FIG. 1. Schematic representation for the hydroxylation of BNNSs.

immediately transferred into a BNNSs dispersion at room temperature under stirring. Next, 1.2-g iron powder and 50 mL 0.5 mol·mL^{-1} HCl were added into the mixture successively and the reaction was kept for 2 h to obtain the target product. The product was washed with deionized water and methanol to remove the excess diazonium salt. In order to ensure impurities were fully removed, the product was extracted by a set of Soxhlet apparatus with refluxing ethanol for 4 h. The product was dried at 60°C for 24 h in a vacuum oven and named as A-BNNSs. The scheme was shown as Fig. 2.

Synthesis of SC-BNNSs. The aniline decorated A-BNNSs were used as one of raw materials to prepare aliphatic chain grafted BNNSs. First, 6 g A-BNNSs and 0.48 mL pyridine was dispersed in the anhydrous N,N-Dimethylformamide (DMF), 10-g stearyl chloride was dissolved into the anhydrous dichloromethane respectively and stirred for 1 h with an ice bath. Next, the ice bath was removed after the stearyl chloride was added dropwise into the dispersion. Then, the mixture was stirred at room temperature for 12 h. Finally, the resultant product was purified with water to remove the excess unreacted stearyl chloride. The product was dried at 60°C for 24 h in a vacuum oven and named as SC-BNNSs. The scheme was shown as Fig. 3.

Preparation of HDPE/SC-BNNSs nanocomposites

HDPE/SC-BNNSs nanocomposites and HDPE/BNNSs nanocomposites were fabricated using Rheomix OS. The melt-blending process was conducted at 200°C and 50 rpm for 10 min. Mixture of irganox 1010 and 168 was used as an antioxidant in the process.

Characterization

Fourier Transform infrared spectroscopy (FTIR) characterization of BNNSs was carried out using a Perkin-Emler System 2000 infrared spectrum analyzer from American Thermo Fisher company, in the wave number range of 4,000–650 cm^{-1} with KBr pellets. X-ray photoelectron spectroscopy (XPS) data were obtained with an ESCALAB250XI electron spectrometer from American VG company, using 300 W Al Kα radiation. The base pressure is

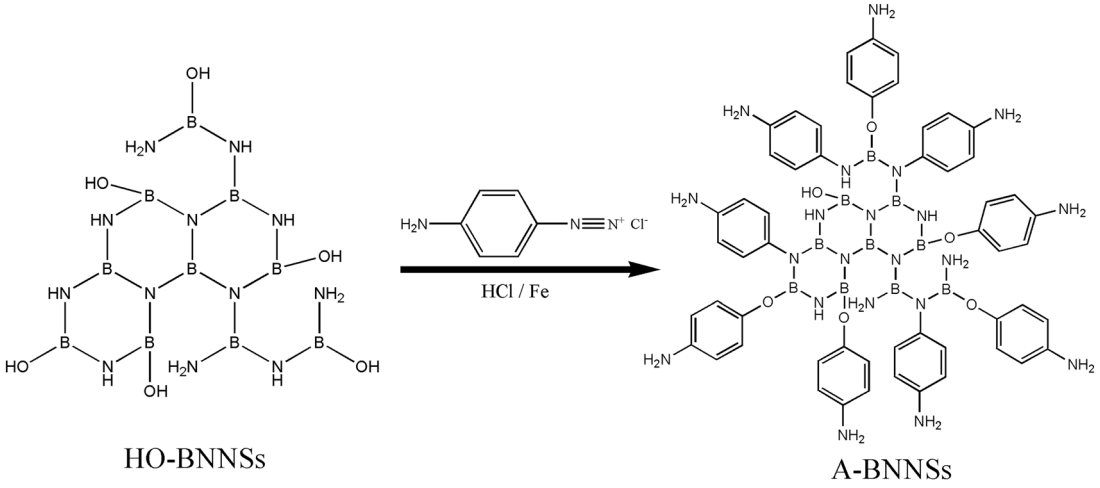

FIG. 2. Schematic representation for the amination of HO-BNNSs.

 DOI 10.1002/pc

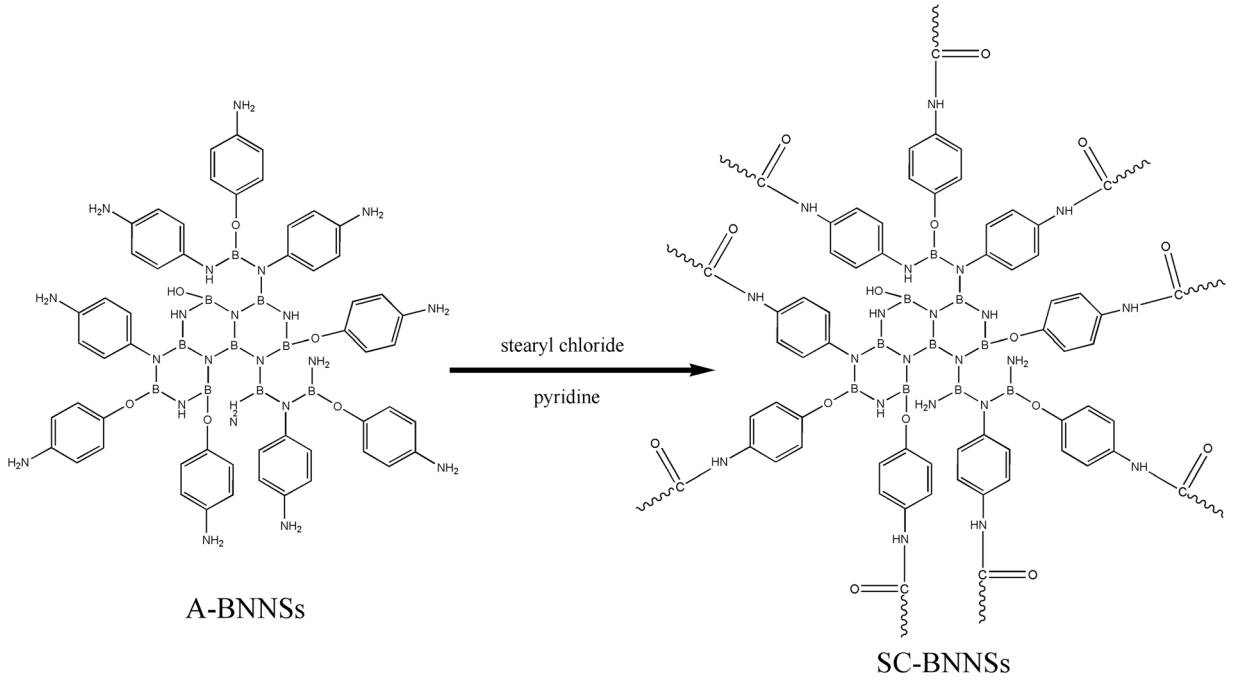

FIG. 3. Schematic representation for the amidation of A-BNNSs.

about 3×10^{-9} mbar. The binding energies are referenced to the C1s line at 284.6 eV from adventitious carbon. The thermal stability of the composites was characterized by Pyris 1 TGA AIR thermogravimetric analyzer (TGA) from American PE company. The thermal behavior was characterized by temperature programming from 50 to 700°C at a heating rate of 10°C·min^{-1}. The content of the grafted functional groups was calculated by thermogravimetric loss between 250 and 600°C. Scanning electron microscope (SEM) image was taken on a SU8020 field emission scanning electron microscope from Japanese Hitachi company at 10 kV. The specimen of SEM was fractured in liquid nitrogen. The fractured surfaces were coated with Pt to enhance the conductivity before the SEM observation.

Thermal transmission property of nanocomposites was assessed using a LFA 447 thermal conductivity instrument from German NETZSCH according to the ASTM E-1461 standard. The effective thermal conductivity κ was calculated according to the following equation (*Eq. 1*):

$$\kappa = T_d \times d \times C_p \tag{1}$$

where T_d, d and C_p are thermal diffusivity (mm^2·s^{-1}), density (g·cm^{-3}) and specific heat capacity (J·kg^{-1}·K^{-1}), respectively. κ, T_d, and C_p could be directly calculated by the instrument. Bulk density, d, was determined using the weight and volume of a composite specimen with dimensions of ϕ 12.7 × 1 mm. The average bulk density obtained from five measurements was used to minimize errors in the effective thermal conductivity experiment.

Radiation shielding characteristic was determined using thermal neutron transmission instrument from Chinese nuclear instrument factory. Am-Be neutron used as the test radiation source, was placed at the end of cylindrical window-oriented detector side in the paraffin box. The shadow cone excludes the scattered neutrons through atmosphere and indoor. The distance between the neutron resource and the specimen was 17 cm and the distance between the neutron resource and the detector was 30 cm. A Schematic diagram of neutron shielding performance test is shown in Fig. 4 [29]. The specimens with dimensions of diameter 10 cm and 1-cm thickness were prepared via hot processing at 180°C and 10 MPa for 10 min.

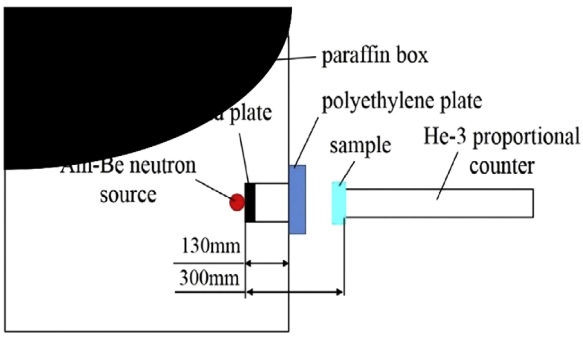

FIG. 4. Schematic diagram of neutron shielding performance test. Reprinted from [23]. [Color figure can be viewed at wileyonlinelibrary.com]

Mechanical properties of nanocomposites were evaluated at 23°C temperature by using a 3365 tensile machine from American INSTRON company. Tensile examinations were carried out according to ISO 527-2. The rate of elongation was 50 mm·min^{-1} and the measurement was repeated five times per specimen. Bending examinations were carried out according to ISO 178:199. The rate of bending was 2 mm·min^{-1} and the measurement was repeated five times per specimen.

RESULTS AND DISCUSSION

Characterization of Modified BNNSs

Characterization of HO-BNNSs. Figure 5 shows the FTIR spectra and XPS spectra of BNNSs and HO-BNNSs. As seen from the Fig. 5a, BNNSs exhibited two distinct peaks at 1,361 and 813 cm^{-1}, which were attributed to B-N stretching (in-plane ring vibration, E_{1u} mode) and B-N-B bending (out-of-plane vibration, A_{2u} mode) [30–32]. However, compared with BNNSs, the peak at 3,427 cm^{-1} which belonged to the hydroxyl group of B-OH, grew much stronger in the HO-BNNSs FTIR spectrum. For XPS spectra, the high-resolution scans of BNNSs and HO-BNNS presented a typical B-N peak at 190.1 eV (B1s) and 398.04 eV (N1 s), respectively [23,30]. Also, it is noticed that a small peak (B-OH) at 191.3 eV appeared in BNNSs and HO-BNNSs. However, the B-OH peak of HO-BNNSs grew larger than that of BNNSs, and the O/B ratio of HO-BNNSs increased to 0.42, which was much higher than that of BNNSs (0.06), indicating that more B components were exposed to B-OH environment in the process of hydroxylation. At the same time, the new peak of the HO-BNNSs located at 399.26 eV (N1 s) was assigned to N-H[33]. It's concluded that the hydroxylation process successfully introduced more B-OH and N-H on the surface of BNNSs.

Characterization of A-BNNSs and SC-BNNSs. Figure 6 shows the FTIR spectra, XPS spectra and TGA curves of BNNSs, A-BNNSs, and SC-BNNSs. Main IR peaks, corresponding literature values and their assignments of HO-BNNSs, A-BNNSs, and SC-BNNSs were given in Table 1 for comparison. As shown in Fig. 6a, besides the B-N stretching and B-N-B bending peaks, some new peaks were observed in FTIR spectra of A-BNNSs and SC-BNNSs. As for A-BNNSs, the absorption peak at 3,378 cm^{-1} belonged to N-H stretching vibration of the amino group; the peak at 1,615 cm^{-1} was assigned to N-H bending vibration of primary amine, indicating that aniline was successfully grafted to the surface of BNNSs. As for SC-BNNSs, the absorption peak at 3,422 cm^{-1} belonged to N-H stretching vibration of secondary amide; peaks at 2,925 and 2,849 cm^{-1} were assigned to C-H aliphatic stretch, the peak at 1,665 cm^{-1} belonged to C=O stretching vibration, revealing that stearyl chloride was successfully reacted with A-BNNSs. The element content from XPS for BNNSs, A-BNNSs and SC-BNNSs were also summarized in Table 2. When compared with BNNSs, the content of C element in A-BNNSs and SC-BNNSs increased by 17.07 and 50.06%, respectively. The increased C content originated from the aniline and aliphatic chains of A-BNNSs and SC-BNNSs, respectively. In addition, in Fig. 6b and c, two new peaks of A-BNNSs located at 191.9 eV (B1s) and at 399.4 eV (N1 s) were

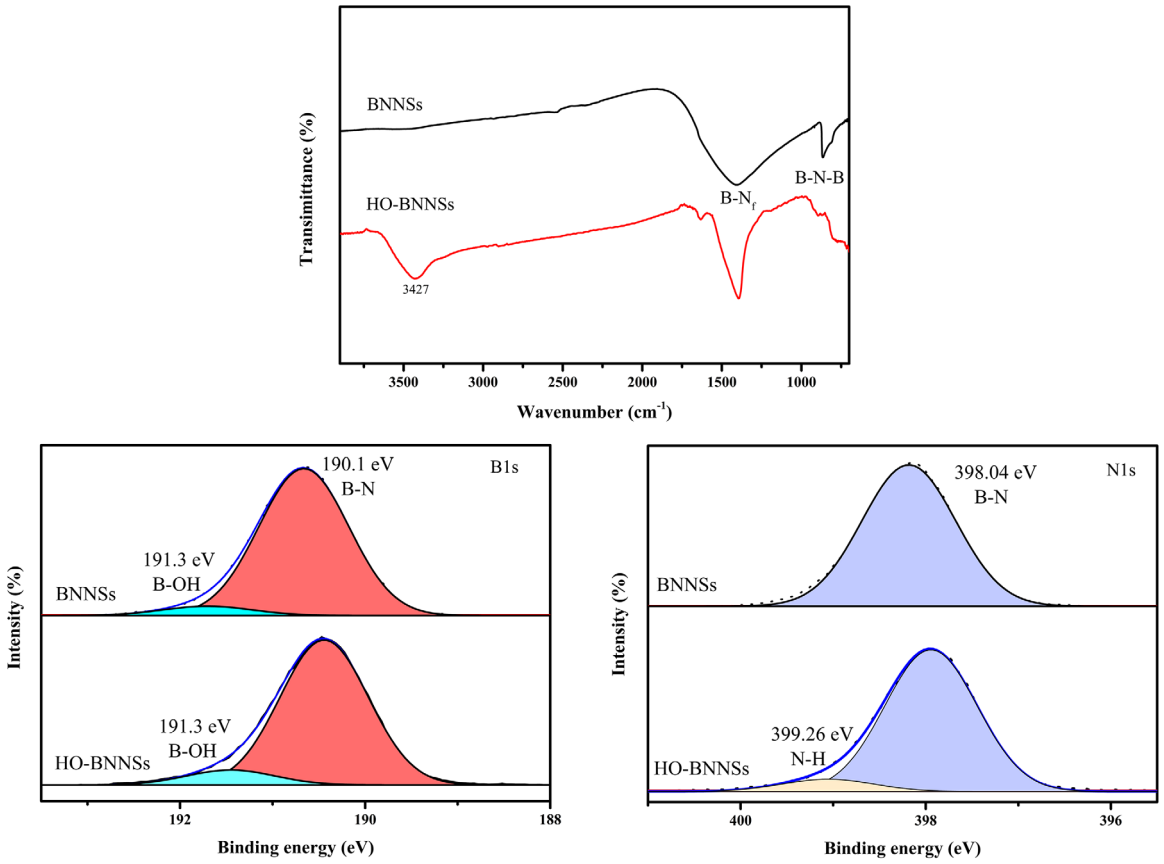

FIG. 5. FTIR spectra, B1s, and N1 s spectra of BNNSs and HO-BNNSs. [Color figure can be viewed at wileyonlinelibrary.com]

 DOI 10.1002/pc

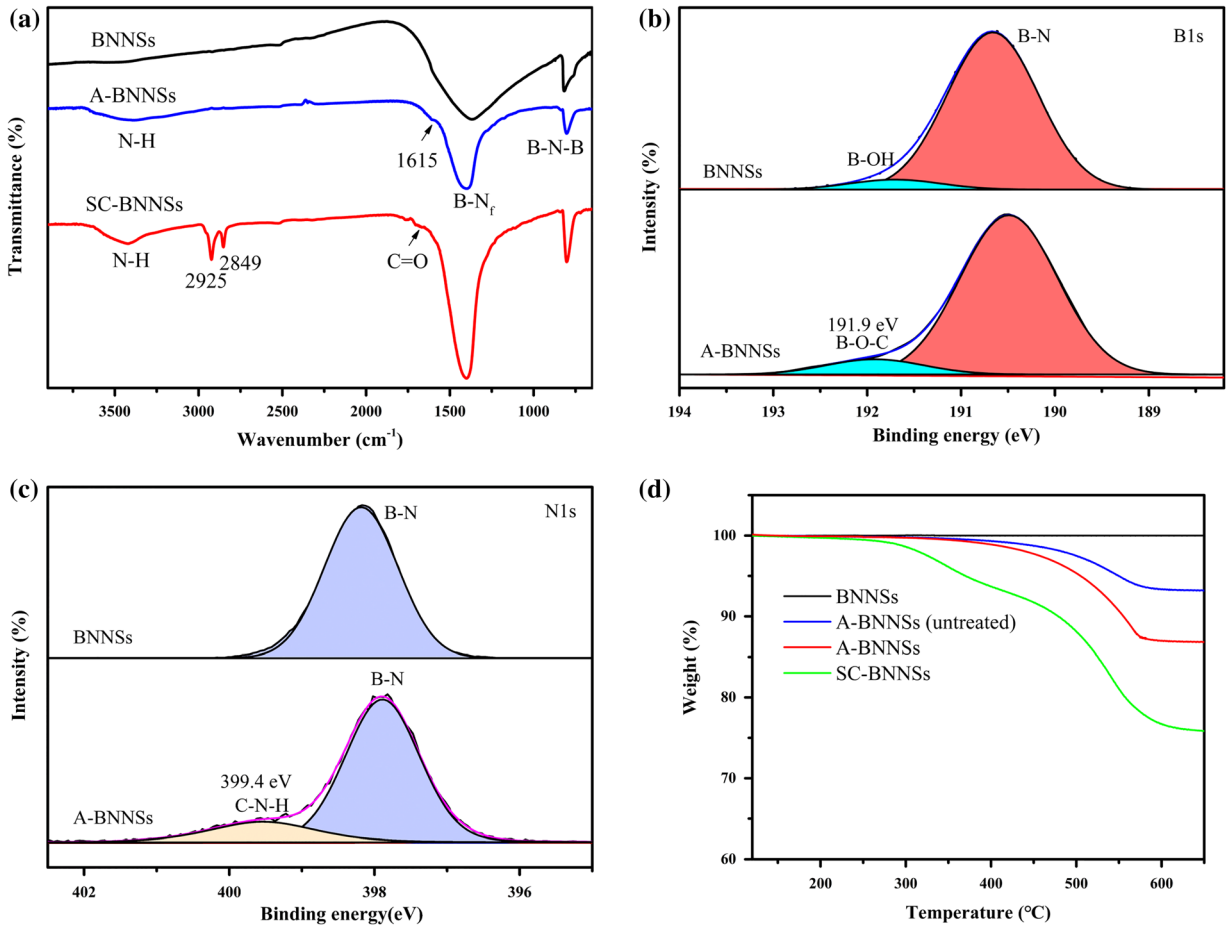

FIG. 6. FT-IR spectra (a), B1s (b), N1 s (c), and TGA curves (d) of BNNSs, A-BNNSs and SC-BNNSs. [Color figure can be viewed at wileyonlinelibrary.com]

TABLE 1. The main characteristic peak values of HO-BNNSs, A-BNNSs and SC-BNNSs.

Sample types	FTIR peak values (cm^{-1})	Reference values (cm^{-1})	Assignments
HO-BNNSs	1,361	1,353	$\beta_{B\text{-}Nf}$
	813	809	$\gamma_{B\text{-}N\text{-}B}$
	3,427	3,500–3,300	$\nu_{O\text{-}H}$ of B-OH
A-BNNSs	3,378	3,500–3,300	$\nu_{N\text{-}H}$ of amine group
	1,615	3,100–3,000	$\nu_{N\text{-}H}$ of primary amine
	1,361	1,353	$\beta_{B\text{-}Nf}$
	813	809	$\gamma_{B\text{-}N\text{-}B}$
SC-BNNSs	3,422	3,540–3,180	$\nu_{N\text{-}H}$ of secondary amide
	2,925 and 2,849	2,930 and 2,850	$\nu_{C\text{-}H}$ of aliphatic chain
	1,665	1690~1630	$\nu_{C=O}$ of amide I band
	1,361	1353	$\beta_{B\text{-}Nf}$
	813	809	$\gamma_{B\text{-}N\text{-}B}$

TABLE 2. The concentration of each element from XPS for BNNSs, A-BNNSs, and SC-BNNSs.

	Chemical composition (at.%)			
Samples	B 1 s	N 1 s	C 1 s	O 1 s
BNNSs	49.34	42.79	4.09	3.78
A-BNNSs	38.69	35.47	21.16	4.68
SC-BNNSs	19.5	19.95	54.15	6.4

ascribed to B-O-C and C-N-H, respectively, which were both resulted from the grafting of aniline groups. Therefore, based on surface activated BNNSs, aniline groups were attached to generate A-BNNSs via reacting with the diazonium salt. Further the stearyl chloride could effectively react with the surface aniline group of A-BNNSs to obtain aliphatic chain grafted BNNSs.

TGA analysis was applied to evaluate the grafting content of the organic component. In the Fig. 6d, there was

almost no heat loss of BNNSs due to its excellent high temperature thermal stability. Importantly, the weight loss of A-BNNSs (12.21 wt%) was higher than that of untreated A-BNNSs (6.74 wt%), which means that the hydroxylation of BNNSs could increase the grafting content of aniline groups. In addition, the organic component of SC-BNNSs was calculated as 22.9 wt%, with the grafting content of stearyl chloride at 10.7 wt% thanks to abundant aniline groups on the surface of A-BNNSs. The TGA analysis confirmed the advantage of the hydroxylation process and the high reactivity of carbocation could ensure the high grafting yield of aniline groups thus further attribute to the aliphatic chain decoration.

The surface morphology of BNNSs, A-BNNSs and SC-BNNSs were also investigated. As shown in Fig. 7a, the original BNNSs had a smooth and flat surface. The average particle size was about 300 nm and the average thickness was 30–120 nm. On the contrary, A-BNNSs and SC-BNNSs had a rough surface due to the grafting of organic anilines and aliphatic chains, respectively. Additionally, the morphology of A-BNNSs changed little compared with naked BNNSs, indicating the hydroxylation process did not destroy the main intrinsic structure of BNNSs.

Nanocomposites Characterization

Distribution of Fillers in HDPE. Figure 8 showed SEM micrographs of the fractured surface of HDPE/BNNSs nanocomposites and HDPE/SC-BNNSs nanocomposites with different amounts of fillers. In HDPE/BNNSs nanocomposites, many agglomerated BNNSs regions were observed when the filler addition was 3 wt% and the agglomeration became more serious as the filler content increased. The intrinsic agglomeration property of nanometer particles was evident in polyethylene matrix. A plenty of interfacial voids were also observed at the interface of the HPDE and BNNSs, indicating that the compatibility between unmodified BNNSs and HDPE was very poor. However, in Fig. 8b, there was an extremely uniform distribution of SC-BNNSs in the nanocomposites when the SC-BNNSs amount was 0.5 wt%. Even when the amount increased to 10 wt%, the distribution of SC-BNNSs in HDPE was still uniform and the agglomeration could hardly be observed on fractured surfaces of the HDPE/SC-BNNSs nanocomposites. The surface aliphatic chain of SC-BNNSs decreased the interfacial voids at the interface and increased the interfacial affinity between the HDPE matrix and SC-BNNSs. Therefore, surface modification of nano-fillers could apparently improve the dispersibility of SC-BNNSs in the HDPE matrix.

Thermal endurance properties. TGA curves revealed the thermal stability of nanocomposites by showing their decomposition characteristics. According to Fig. 9a and b. compared with the neat HDPE, the 0.5 and 1 wt% additive amount of BNNSs and SC-BNNSs both had little impact on the thermal decomposition temperature of HDPE. When 5 and 10 wt% of SC-BNNSs and BNNSs were added to HDPE, the thermal stability of HDPE improved obviously. However, there were differences between two kinds of fillers in regard to the thermal stability enhancement of HDPE. As for the 10 wt% addition of fillers, when the decomposition of nanocomposites amounted to 10%, the thermal decomposition temperature of nanocomposites both increased by about 50°C; But when the decomposition of HDPE/SC-BNNSs nanocomposites (10 wt% fillers) amounted to 80%, the thermal decomposition temperature of HDPE increased by about 150°C, much higher than that of BNNSs, which only postponed the temperature for nearly 50°C. Therefore, the surface modification of BNNSs apparently increased the thermal stability of HDPE, especially during the late stage of the degradation process, which exhibited improved enhancement than naked BNNSs. We supposed that the entangling association between the polyethylene molecular chains and the surface aliphatic chains of SC-BNNSs facilitated the thermal endurance property of HDPE/SC–BNNSs nanocomposites.

Thermal Conductivity and Neutron-Shielding Properties. Thermal conductivities of HDPE/SC-BNNSs nanocomposites and HDPE/BNNSs nanocomposites are showed in Fig. 10a. Thermal conductivity of the nuclear radiation shielding materials is an important issue, because the thermal conductive materials are helpful for releasing the heat generated from nuclear reactors [3,34]. The neat HDPE had thermal conductivity of 0.508 $W \cdot m^{-1} \cdot K^{-1}$. The addition of BNNSs and SC-BNNSs fillers increased the effective thermal conductivity, featuring climbing lines with the increasing filler content. And HDPE/SC-BNNSs nanocomposites represented much higher thermal conductivity than those of HDPE/BNNSs nanocomposites. The surface modification of BNNSs led to

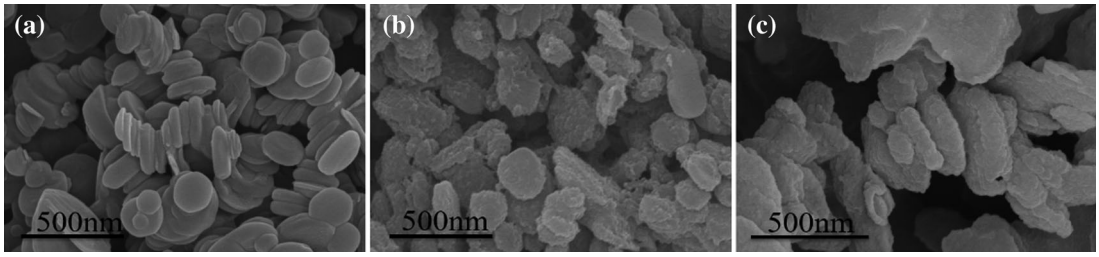

FIG. 7. SEM images of (a) BNNSs (b) A-BNNSs, and (c) SC-BNNSs.

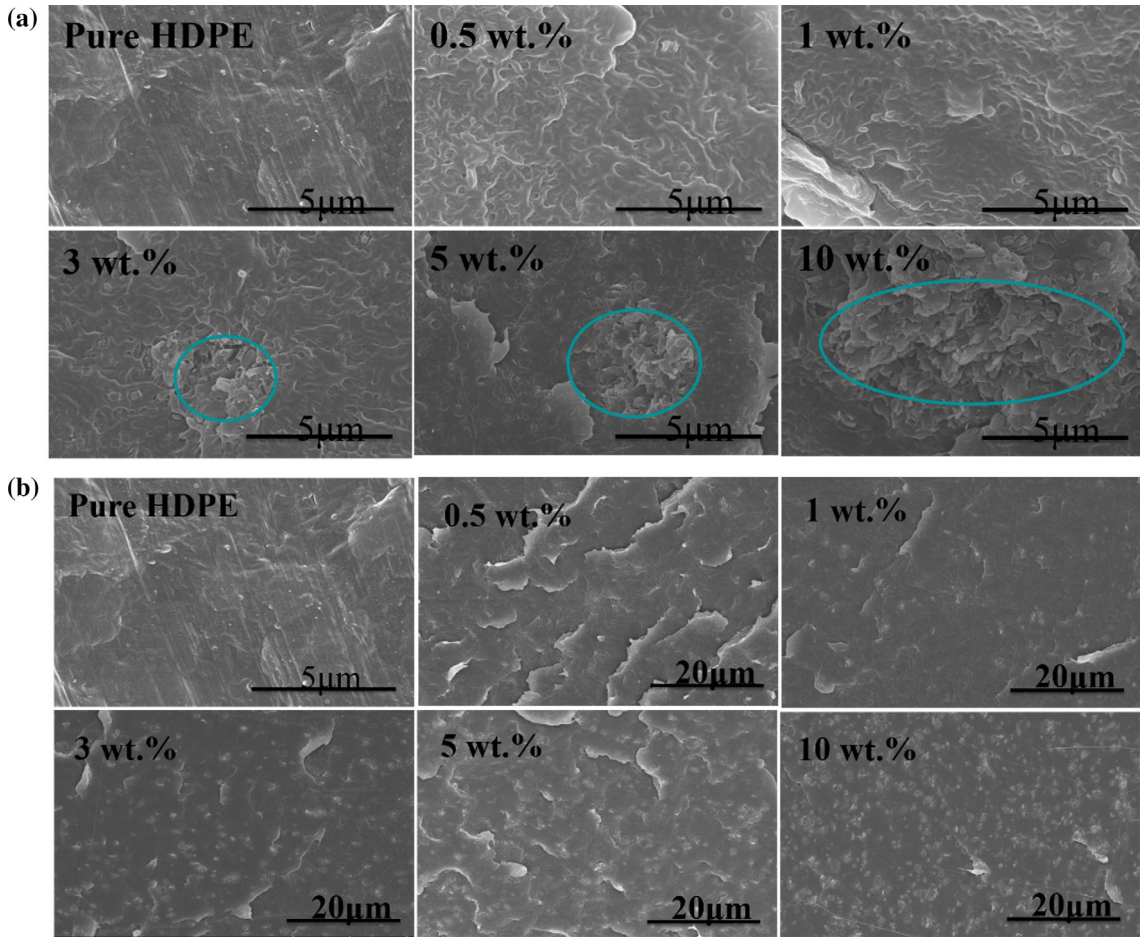

FIG. 8. SEM micrographs of the fractured surface of (a) HDPE/BNNSs nanocomposites and (b) HDPE/SCBNNSs nanocomposites. [Color figure can be viewed at wileyonlinelibrary.com]

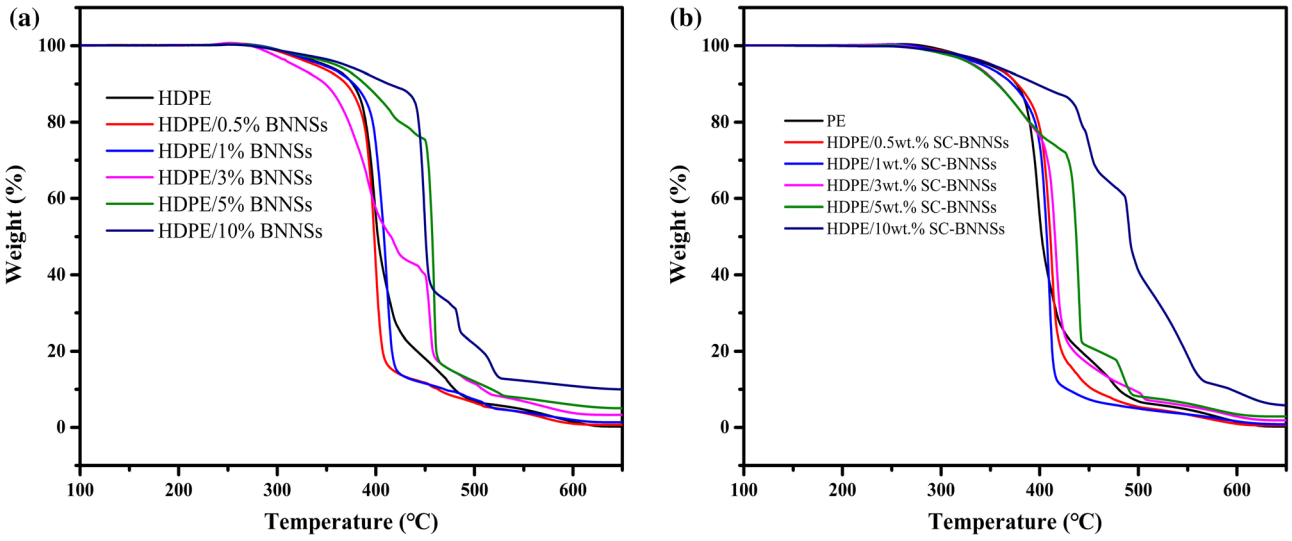

FIG. 9. TGA curves for (a) HDPE/BNNSs nanocomposites and (b) HDPE/SC-BNNSs nanocomposites. [Color figure can be viewed at wileyonlinelibrary.com]

a meaningful improvement of the effective thermal conductivity. Generally, the phonon scattering at the interface of matrix/filler restricts heat transfer and a poor interfacial adhesion between the matrix and the fillers leading to a large phonon scattering [35]. The surface functionalization of fillers attributed to an alleviated phonon scattering at the interface of HDPE matrix and SC-BNNSs particles, compared with that of HDPE/BNNSs nanocomposites [29].

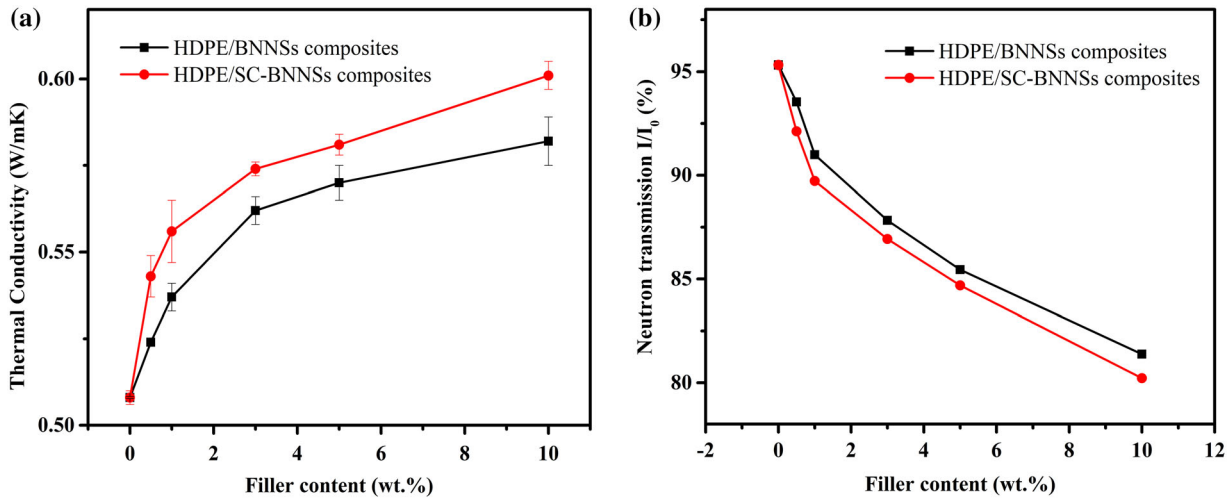

FIG. 10. Effective thermal conductivity (a) and Neutron transmission factor (b) for HDPE/SC-BNNSs nanocomposites and HDPE/BNNSs nanocomposites, respectively. [Color figure can be viewed at wileyonlinelibrary.com]

Figure 10b represents the neutron flux attenuation properties of 10-mm thick nanocomposites. The neutron transmission factor I/I_0 was used to assess the neutron shielding properties, where I_0 and I are the intensities of incident neutron beam and neutron beam transmitted through the thickness direction of the sample nanocomposites, respectively [29]. The neat HDPE materials were ~95%. As the BN content of nanocomposites increased, the neutron transmission factor decreased. When the content of SC-BNNSs was 10 wt%, the neutron transmission factor decreased by 15.8% lower than the pure HDPE. The HDPE/SC-BNNSs nanocomposites revealed a higher neutron radiation shielding efficiency than the HDPE/BNNSs nanocomposites. As shown in the above SEM images, the surface modified BNNSs in the HDPE matrix represented a comparatively better dispersion and stronger interfacial adhesion than the unmodified one, which effectively enhanced the neutron shielding ability.

Mechanical Properties. Figure 11 shows flexural modulus and tensile strength of HDPE/SC-BNNSs nanocomposites and HDPE/BNNSs nanocomposites. The flexural modulus increased as the filler content added. When the content of SC-BNNSs was 10 wt%, the flexural modulus of HDPE/SC-BNNSs nanocomposites increased by 38.2% higher than the pure HDPE because the addition of filler increased the rigidity of the sample. Meanwhile, the flexural modulus of HDPE/SC-BNNSs nanocomposites was higher than those of the HDPE/BNNSs nanocomposites because the surface aliphatic chains of SC-BNNSs

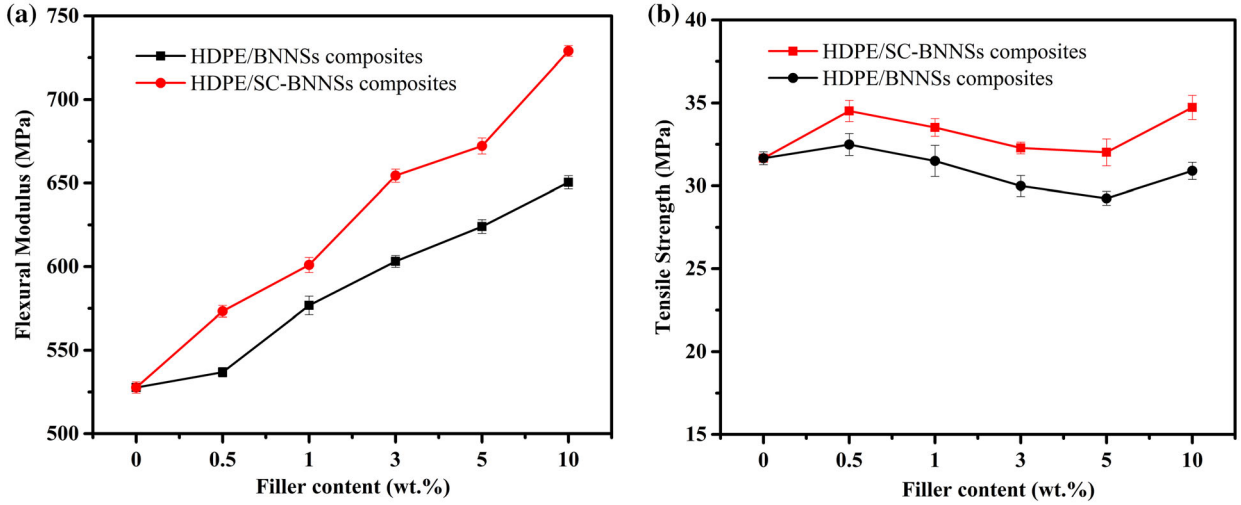

FIG. 11. Flexural modulus (a) and Tensile strength (b) for HDPE/SC-BNNSs nanocomposites and HDPE/BNNSs nanocomposites, respectively. [Color figure can be viewed at wileyonlinelibrary.com]

DOI 10.1002/pc

improved the interfacial adhesion between the filler and HDPE matrix. In addition, as the filler concentration increased, the tensile strength of both nanocomposites initially increased and then decreased. As a small amount of filler powder in the matrix could reinforce the HDPE, the tensile strength of both nanocomposites increased. However, more defects in the matrix appeared when the filler content increased and the tensile strength of nanocomposites were weakened by defects. The tensile strength of HDPE/SC–BNNSs nanocomposites were higher than those of the unmodified nanocomposites, which might result from that the SC-BNNSs fillers modified by aliphatic chains constructed a network among linear polymer chains [36,37].

CONCLUSIONS

An effective method was introduced to break B-N bonds on the surface of BNNSs and generate more B-OH and N-H groups, which were utilized to graft aniline groups by aniline carbocation generated by decomposition of diazonium salt. An amide reaction between A-BNNSs and stearyl chloride verified the reactivity of Ph-NH_2 on the surface of A-BNNSs and provided boron nitride surface aliphatic chains with 22.9 wt% grafting yield. HDPE/SC-BNNSs nanocomposites were fabricated through conventional melt-extrusion to prove the advantages of SC-BNNSs. The surface aliphatic chains of SC-BNNSs filler strongly improved the interfacial adhesion between the polymer matrix and the filler and provided a uniform distribution of SC-BNNSs in the HDPE matrix. The neutron shielding ability and thermal conductivity of HDPE/SC-BNNSs nanocomposites were both obviously improved compared with HDPE/BNNSs nanocomposites. Moreover, the flexural modulus of HDPE/SC-BNNSs nanocomposites was also enhanced while their tensile strength were not apparently weakened. In addition, when the SC-BNNSs content was over 5 wt%, HDPE/SC-BNNSs nanocomposites showed enhanced thermal stability.

ACKNOWLEDGMENTS

This work was supported by the National Science Foundation of China (Grant number: 51403216), PetroChina Innovation Foundation, and the Seed Foundation of Innovation and Creation for Graduate Students in Northwestern Polytechnical University (Grant number: 2017207).

REFERENCES

1. C.M. Parish, K. Wang, and P. D. Edmondson, *Scr. Mater.*, **143**, 169 (2018).
2. H. Berger, *Annual Review of Nuclear Science*., **21**, 335 (1971).
3. K. Okuno, *Radiation Protection Dosimetry*., **115**(1–4), 258 (2005).
4. M.A. Kiani, S.J. Ahmadi, M. Outokesh, R. Adeli, and A. Mohamrnadi, *Radiation Physics and Chemistry.*, **141**, 223 (2017).
5. V.P. Singh, M.E. Medhat, N.M. Badiger, and A.M.S. Rahman, *Radiation Physics and Chemistry.*, **106**, 175 (2015).
6. A. Kommling, K. von der Ehe, D. Wolff, and M. Jaunich, *Radiation Physics and Chemistry*., **142**, 29 (2018).
7. S.A. Thibeault, J.H. Kang, G. Sauti, C. Park, C.C. Fay, and G.C. King, *Mrs Bulletin*., **40**(10), 836 (2015).
8. V.A. Artem'ev, *Atom. Energy.*, **94**(4), 282 (2003).
9. H. Loria, P. Pereira-Almao, and C.E. Scott, *Ind. Eng. Chem. Res.*, **50**(14), 8529 (2011).
10. J. Li, R. Dahal, S. Majety, J.Y. Lin, and H.X. Jiang, *Nuclear Instruments & Methods in Physics Research Section a-Accelerators Spectrometers Detectors and Associated Equipment*., **654**(1), 417 (2011).
11. J.W. Krumpfer, T. Schuster, M. Klapper, and K. Mullen, *Nano Today*., **8**(4), 417 (2013).
12. Z.Y. Zheng, M. Cox, and B. Li, *Journal of Materials Science*., **53**(1), 66 (2018).
13. Y.S. Xu and D.D.L. Chung, *Composite Interfaces*., **7**(4), 243 (2000).
14. Z. Cui, A.J. Oyer, A.J. Glover, H.C. Schniepp, and D. H. Adamson, *Small*., **10**(12), 2352 (2014).
15. C. Zhi, N. Hanagata, Y. Bando, and D. Golberg, *Chem-Asian J.*, **6**(9), 2530 (2011).
16. L. Fu, T. Wang, J.H. Yu, W. Dai, H.Y. Sun, Z.D. Liu, R. Sun, N. Jiang, A.M. Yu, and C.T. Lin, *2d Mater.*, **4**(2), 02547 (2017).
17. A. Pakdel, Y. Bando, and D. Golberg, *Acs Nano*., **8**(10), 10631 (2014).
18. T. Ikuno, T. Sainsbury, D. Okawa, J.M.J. Frehet, and A. Zettl, *Solid State Communications*., **142**(11), 643 (2007).
19. T. Sainsbury, A. Satti, P. May, Z. Wang, I. McGovern, Y.K. Gun'ko, and J. Coleman, *Journal of the American Chemical Society*., **134**(45), 18758 (2012).
20. K. Kim, M. Kim, Y. Hwang, and J. Kim, *Ceramics International*., **40** (1), 2047 (2014).
21. K. Kim, H. Ju, and J. Kim, *Polymer*., **91**, 74 (2016).
22. X.J.J. Dai, Y. Chen, Z.Q. Chen, P.R. Lamb, L.H. Li, J. du Plessis, D.G. McCulloch, and X.G. Wang, *Nanotechnology*., **22**(24), 245301 (2011).
23. R. Jan, P. May, A.P. Bell, A. Habib, U. Khan, and J.N. Coleman, *Nanoscale*., **6**(9), 4889 (2014).
24. M. Yi, Z. Shen, W. Zhang, J. Zhu, L. Liu, S. Liang, X. Zhang, and S. Ma, *Nanoscale*., **5**(21), 10660 (2013).
25. M. Yi, Z. Shen, X. Zhao, S. Liang, and L. Liu, *Appl Phys Lett*., **104**(14), 143101 (2014).
26. M. Yi, Z. Shen, L. Liu, and S. Liang, *Rsc Advances*., **5**(4), 2983 (2015).
27. C. Harrison, S. Weaver, C. Bertelsen, E. Burgett, N. Hertel, and E. Grulke, *Journal of Applied Polymer Science*., **109**(4), 2529 (2008).
28. X.L. Zhang, M. Yang, X.M. Zhang, H. Wu, S.Y. Guo, and Y. Z. Wang, *Composites Science and Technology*., **150**, 16 (2017).
29. H. Chai, X. Tang, M. Ni, F. Chen, Y. Zhang, D. Chen, and Y. Qiu, *Journal of Nuclear Materials*., **464**, 210 (2015).

30. E. Chigo Anota, Y. Tlapale, M. Salazar Villanueva, and J. A. Rivera Marquez, *Journal of Molecular Modeling*., **21**(8), 215 (2015).
31. I.M. Joni, R. Balgis, T. Ogi, T. Iwaki, and K. Okuyama, *Colloids and Surfaces a-Physicochemical and Engineering Aspects*., **388**(1–3), 49 (2011).
32. H.-B. Cho, Y. Tokoi, S. Tanaka, H. Suematsu, T. Suzuki, W. Jiang, K. Niihara, and T. Nakayama, *Composites Science and Technology*., **71**(8), 1046 (2011).
33. T. Sugino, T. Tai, and Y. Etou, *Diamond and Related Materials*., **10**(3–7), 1375 (2001).
34. Y. Huang, W. Zhang, L. Liang, J. Xu, and Z. Chen, *Chemical Engineering Journal*., **220**, 143 (2013).
35. J.P. Hong, S.W. Yoon, T.S. Hwang, Y.K. Lee, S.H. Won, and J.D. Nam, *Korea-Aust. Rheol. J*., **22**(4), 259 (2010).
36. J. Kim, B.C. Lee, Y.R. Uhm, and W.H. Miller, *Journal of Nuclear Materials*., **453**(1–3), 48 (2014).
37. M.A. Sharaf and J.E. Mark, *Polymer*., **45**(11), 3943 (2004).

 DOI 10.1002/pc